Chalcogenide Letters Vol. 22, No. 5, May 2025, p. 493 - 506

Preparation and characterization of $CuAl_XSn_{1-X}S_2$ thin films prepared by electron beam deposition system

A. S. Alqarni [a,*], S. N. Alamri [b,*]
[a] *Department of Physics, College of Science, Princess Nourah bint Abdulrahman University, P.O. Box 84428, Riyadh 11671, Saudi Arabia*
[b] *Department of Physics, Faculty of Science, Taibah University, Madinah, Saudi Arabia*

Abundant and environmentally friendly solar cells materials Cu_2AlSnS_4 (CATS) thin film successively prepared by electron beam deposition system. The impact of various deposition times and post-annealing at 450 °C under nitrogen gas atmosphere on the structures, morphologies, and spectroscopic characteristics of the obtained CATS films were investigated. Both deposition time variation and annealing process were found to significantly affect the crystallinity, bonding vibration, surface morphology, energy band gaps, and Urbach energy of the CATS films. EDX spectra of the films disclosed the existence of all constituents' elements. XRD analysis of the post-annealed films verified their multiple phases with varying crystallite sizes. Raman spectral data of these films agreed with the XRD analysis. AFM and SEM images of the films revealed the growth of hemi-spherical crystallites on their surface. The band gap energy of these as deposited and annealed films was correspondingly varied from 1.26 - 1.59 eV and 1.14 - 0.94 eV. The proposed CATS films are asserted to be promising for the advancement of novel solar cell materials.

(Received February 8, 2025; Accepted May 27, 2025)

Keywords: CATS thin film, Electron beam deposition (EBD), Structure, Morphology, Transmittance

1. Introduction

The ever-growing demand of renewable energy has enforced the researchers worldwide to develop high-performance photovoltaic cells that can efficiently convert the solar radiation into electrical power. To speed up the installation of the photovoltaic modules, its production cost and weight must be lowered. To achieve this goal, several thin films made from polycrystalline Cu–Sn–S (CTS) were proposed by different researchers [1-10]. The CTS system can be composed of various phases depending on the synthesis conditions. The phase diagram of CTS [10] obtained at standard temperature and pressure revealed the existence of several stable phases like SnS, SnS_2, Cu_3SnS_4, Cu_2SnS_4 and Cu_2SnS_3. In addition, the solar cell made of CTS with diverse phases were reported [11, 12]. The heterojunction solar cells derived from Cu_2SnS_3 disclosed highly stabile [13, 14] polymorphs phases with tetragonal [15], monoclinic [16], cubic [17], hexagonal [18] and wurtzite [19] crystal structures. The energy band gaps of the CTS film are ranged from 1.4-1.5 eV with an enhanced coefficient of absorption close to 10^4 cm^{-1} [20]. Single-junction solar cells derived from Cu_2SnS_3 displayed a theoretical efficiency of 30% [21]. Conversely, the Cu_2SnS_3 thin films-based Schottky-type solar cells disclosed the value of efficiency about 0.11% [13]. Recently, the thin films-based solar cell made from pristine CTS [22], Na-doped Cu_2SnS_3 [23], Ge-doped Cu_2SnS_3 [24] and Cu_2ZnSnS_4 [25] was shown to attain an efficiency as much as 4.29%, 4.8%, 6.7% and 11%, respectively, compared to theoretical efficiency of 30% [26]. Based on these factors, diverse strategies including doping by various metals [27, 28] have been adopted to improve various features of the solar cells made from quaternary materials, proving their potential for efficiency enhancement. The observed enhancement in the efficiency of metal-doped thin films solar cell was

* Corresponding authors: arsalqarni@pnu.edu.sa
. https://doi.org/10.15251/CL.2025.225.493

mainly due to their diffusion into the absorber material layers. Aluminum (Al) as a promising doping candidate revealed immense prospect in certain thin film solar cell technologies. Incorporating aluminum into thin film compositions for solar cells can improve performance by enhancing conductivity, light absorption, and the structural stability of the films. This makes them more durable and resistant to degradation over time, ultimately resulting in greater efficiency and lifespan for the solar cells [27–33].

Considering the practical importance of CTS system-based solar cells applications, in this work, the abundant, affordable, and non-toxic chemical element Al was incorporated into the CTS thin films. To our knowledge, the quaternary Al-doped CTS films were produced for the first time by electron beam deposition (EBD) technique and characterized using various analytical tools. The obtained data were analyzed, interpreted, discussed, and compared. The deposited thin films were demonstrated to be prospective for the development of efficient photovoltaic cells.

2. Preparation and characterization

In this study, the $CuAl_xSn_{1-x}S_2$ (CATS) thin films were deposited on glass substrates (1.5×3.5 cm^2) at a temperature of 80 ºC. An electron-beam evaporator system with chamber pressure 5×10^{-5} mbar, acceleration potential of 8 kV and 50 mA electron beam current was utilized. The source was a ball-milling powder consisting of pure Copper (Cu, 99.99%), Al (99.99%), Sn (99.99%) and S (99.99%).

The $CuAl_{0.2}Sn_{0.8}S_2$ powder source was weighed according to an atomic ratio of 1: 0.2: 0.8: 2 using a Retsch PM 400 ball mill. The milling time was 18 h in air, with a 10 min pause every 1 h, and the rotation speed was 350 rpm. Tungsten carbide balls with a diameter of 10 mm diameter were used, and the ball-to-powder weight ratio was 15:1. Three films at the deposition time of 3 min, 6 min and 15 min were made. A profile-meter (Veeco dektak 150) was employed for measuring the films' thicknesses.

To ascertain the chemical elemental composition, the energy dispersive X-ray spectrometry (EDX) system coupled with a JEOL scanning electron microscope (SEM, JCM-6000 model) was used. The crystal structures and phases of the samples were determined by X-ray diffractometer (Shimadzu XRD-6000 model with Cu-Kα like of λ = 1.5406 Å), wherein the data was recorded at 2θ ranged from 5° to 80°. In addition, the Raman spectrum of these films was obtained by a Raman spectrometer (Bruker Senterra model, excitation source of 532 nm and precision of 3.5 cm^{-1}). Atomic force microscopy (AFM, Veeco-CP-II model having Si tip at scan frequency of 1 Hz) and Shimadzu scanning electron microscopy (SEM) were used to image the samples topography. An UV–Vis-NIR scanning spectrometer (Shimadzu UV- 3101 PC) was employed to study the transmittance spectra of the CATS film.

All the characterizations of these prepared films were conducted at room temperature before and after the annealing process. First, all the as depsoited CATS films were characterized. Then, these films were annealed at 450 °C for an hour under Nitrogen gas atmosphere. Finally, the post-annealed films were characterized for comparison.

3. Results and discussion

3.1 EDX spectra

Fig. 1 displays the EDX spectrum of the CATS films, which consisted of only Cu, Sn, Al and S peaks, indicating the complete absence of any impurity thereby confirming the purity of the prepared films. The percentages of the constituent elements were obtained by analyzing various points on each film's surface. Table 1 depicts the deduced mean value alongside the elemental composition. The values of S/Metal ratios in the CATS films deposited at 3, 6 and 15 min were correspondingly 1.2, 1 and 0.9% which are consistent with the documented results for typical Cu_2ZnSnS_4 (CTZS) solar cell (in the range of 0.9 to 1.1) performs at optimum efficiency [34].

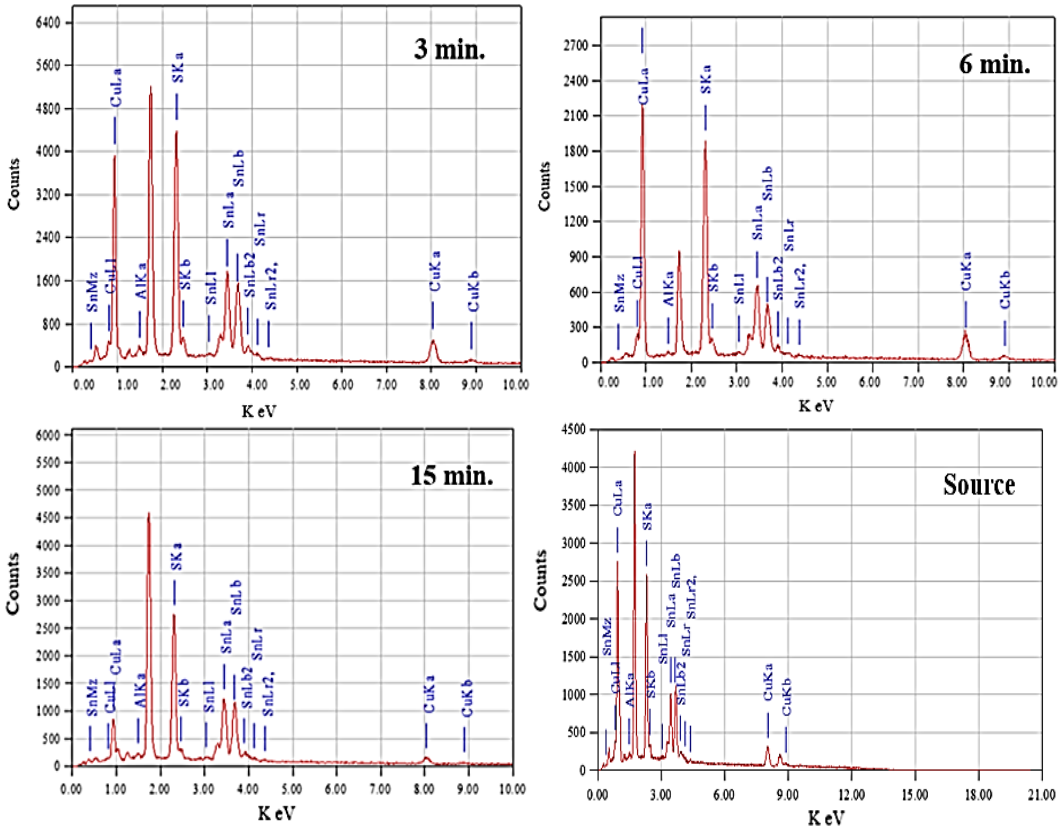

Fig. 1. EDX spectrum of the source powder and deposited CATS thin films.

Table 1. The constituent elements in the powder source and CATS thin films obtained from EDX analysis.

Time (min.)	Atomic composition (%)					Composition
	Cu	Sn	Al	S	S/Metal	
3	12.53	28.49	2.75	56.23	1.28	$Cu_{0.5}\ Al_{0.11}Sn_{1.14}\ S_{2.2}$
6	25.58	21.36	2.98	50.08	1	$Cu_{1.02}\ Al_{0.12}Sn_{0.85}\ S_2$
15	30.84	18.23	1.20	49.72	0.99	$Cu_{1.23}\ Al_{0.05}Sn_{0.73}\ S_2$
Source	25	21.7	2.7	49.77	1	$Cu\ Al_{0.12}Sn_{0.8}\ S_2$

3.2. XRD pattern and Raman spectral analysis of the CATS films

Figs. 2 and 3 illustrate the XRD patterns of CATS films before and after being annealed, respectively. This detected halo at lower angular range without any intense diffraction peaks signified the lack of the long-range periodicity of atoms in the as deposited films (Fig. 2). Conversely, XRD results of the post-annealed CATS films indicated their polycrystallinity (Fig. 3) wherein the observed sharp diffraction peaks at 14.5°, 28.1°, 47.2°, and 56.0° were corresponded to the lattice planer directions of (111), (311), (400), and (620) for tetragonal Cu_2AlSnS_4 unit cell (JCPDS # 00-047-1343) that agreed well with the earlier report [28]. In addition, the diffraction peaks at around 28.1° and 47.2° are due to the corresponding (112) and (220) lattice planes of the tetragonal phase of Cu_2SnS_3 (JCPDS # 01-089-4714) [35]. All the deposited CATS films displayed another crystalline phase of Cu_2S with a minor peak at 31.6° which was also reported by others [4, 35]. All the annealed films showed a minor peak at 21.2° which corresponded to the (103) lattice direction of Sn_2S_3 crystal (JCPDS # 75- 21830) [35].

The observed most significant diffraction peak at 28.1° was analyzed using Debye Scherer equation to calculate the mean crystallite diameter in the films wherein the FWHM of this major peak was recorded [36]. The crystallite sizes in the post-annealed films were decreased from 10.8 to 9.6 nm when the deposition times were raised from 3 - 15 min. In this work, calculated values of

mean crystallite diameters were comparable to the one obtained for CTS film (11.4 nm) prepared using spray pyrolysis method [37] and the one observed for CTS film (10.7 nm) made using co-evaporation method [35].

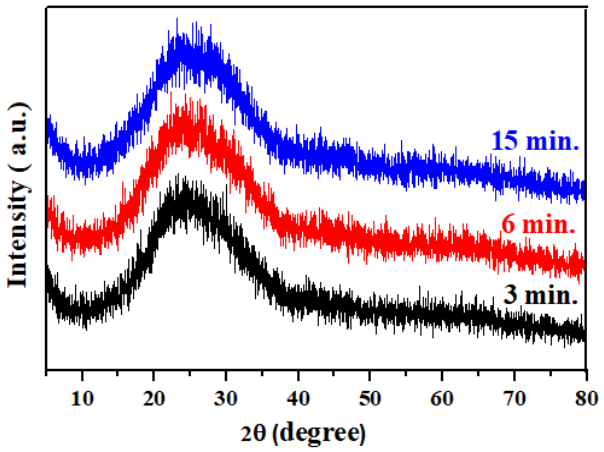

Fig. 2. XRD profiles of as- deposited thin films.

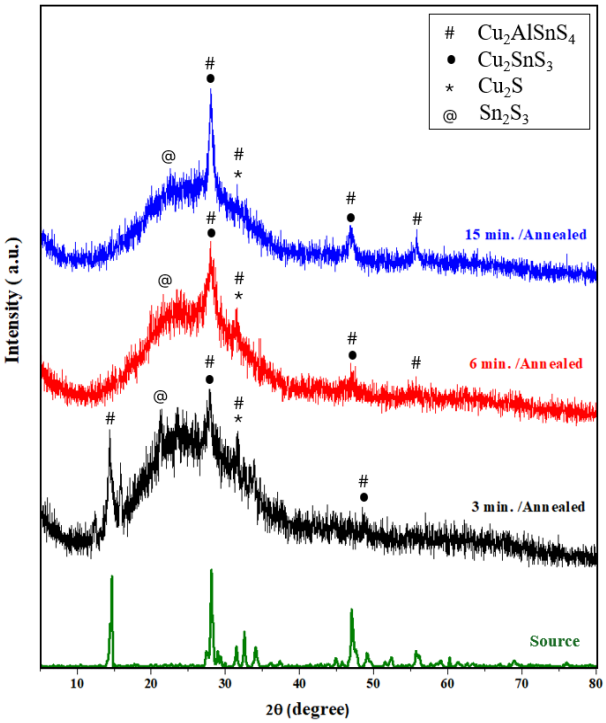

Fig. 3 XRD profiles of post-annealed samples.

Figs. 4 and 5 display the Raman spectrum of the CATS films before and after being annealed, respectively. Overall spectral patterns of these films were changed significantly with the variation of deposition time, indicating some change in the chemical functional groups. Multiphase verification through Raman spectroscopy was achieved by identifying distinct vibrational peaks unique to each phase. Table 2 compares the observed peak positions for CATS films with those reported in the literature. Raman spectral analyses reconfirmed the existence of multiphase in the prepared thin films. The spectra showed the presence of tetragonal Cu_2AlSnS_4, Cu_2SnS_3, Cu_2S and

Sn_2S_3 phases (as observed in the XRD patterns) together with the minor SnS_2 phase. The slight difference in the wavenumber between the observed values and those reported by others are mainly because of the variation of films composition, growth conditions and microstructures [6].

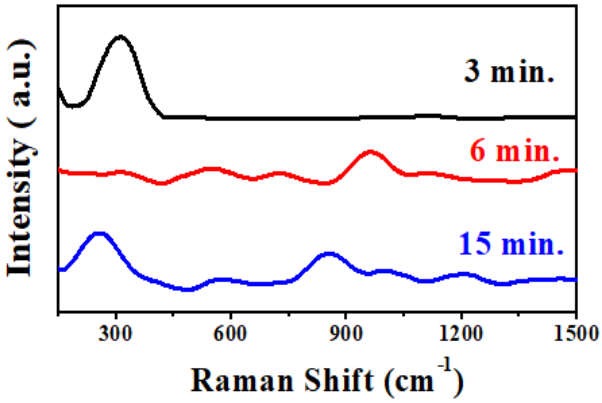

Fig. 4. Raman spectrum of as deposited CATS films.

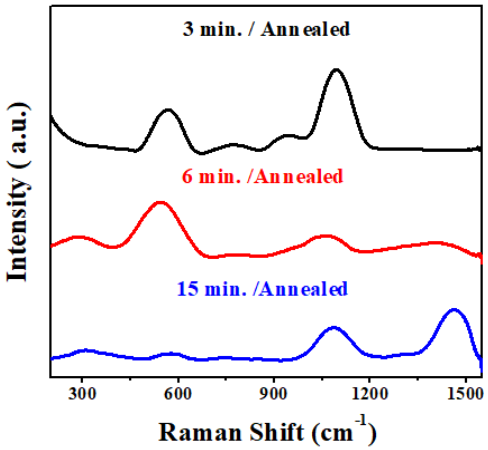

Fig. 5. Raman spectrum of post-annealed CATS films.

Table 2. Comparison of Raman peaks in the current study with other works.

Observed Raman peaks (cm^{-1})							**Reported values (cm^{-1})**
As deposited CATS films				Post-annealed CATS films			
3 min	6 min	15 min		3 min	6 min	15 min	
308	306	260		569	544	567	303 (tetragonal Cu_2SnS_3 [38]) 475 & 492 (Cu_2S [4] & [39]) 536 & 580 (SnS_2 [40])
-	965	858		1093	1066	1084	1379 (Cu_2AlSnS_4 films [42]) & 1370 (Sn_2S_3 [47])
				-	1410	1458	1383 (Cu_2AlSnS_4 films [42])

3.3. Morphological analysis of CATS films

Figs. 6 and 7 depict the corresponding AFM images of the CATS films before and after being annealed. The surface textures of the films were consisting of compact and dense grains without pinholes or cracks, indicating the impact of different times of deposition as well as the

annealing effect on the film's microstructures. Both roughness and size of the observed hemi-spherical grains were improved with the annealing process and deposition time increase from 3 to 6 min and then decreased at 15 min.

The top-view SEM images of the studied films before and after the annealing protocol are epitomized in Figs. 8 and 9, respectively. These images revealed that compact and dense films without pinholes or cracks were successfully obtained at different deposition times. The histogram (inset of Figs. 8 and 9) illustrates the average grain size of the observed semi-spherical grains. Apparently, the grain size of the films was augmented with the progressive increase in the deposition time as well as the annealing temperature increased from 3 to 6 minutes. However, for the film with 15 minutes deposition time, the SEM image confirmed the amorphous nature before the annealing which was consistent with XRD result while its image after annealing exhibited about 258 nm grain size. This observation could be attributed to the polycrystalline structure obtained by XRD and Raman analyses.

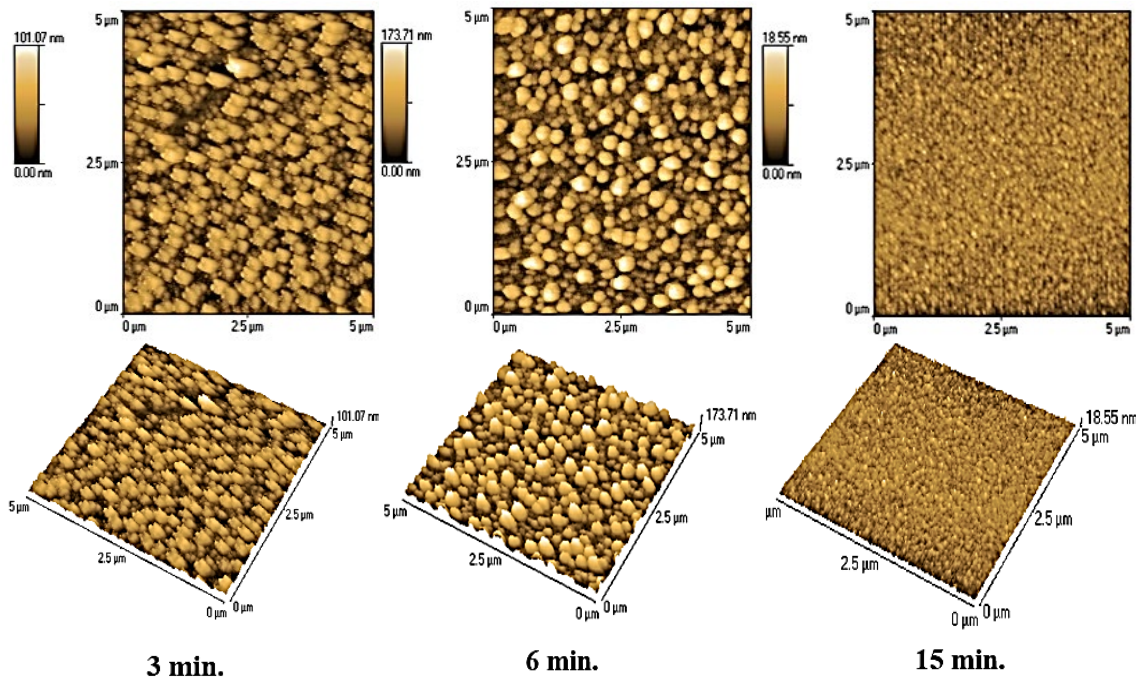

Fig. 6. AFM topographs (in two- and three-dimension view) of as-deposited CATS films.

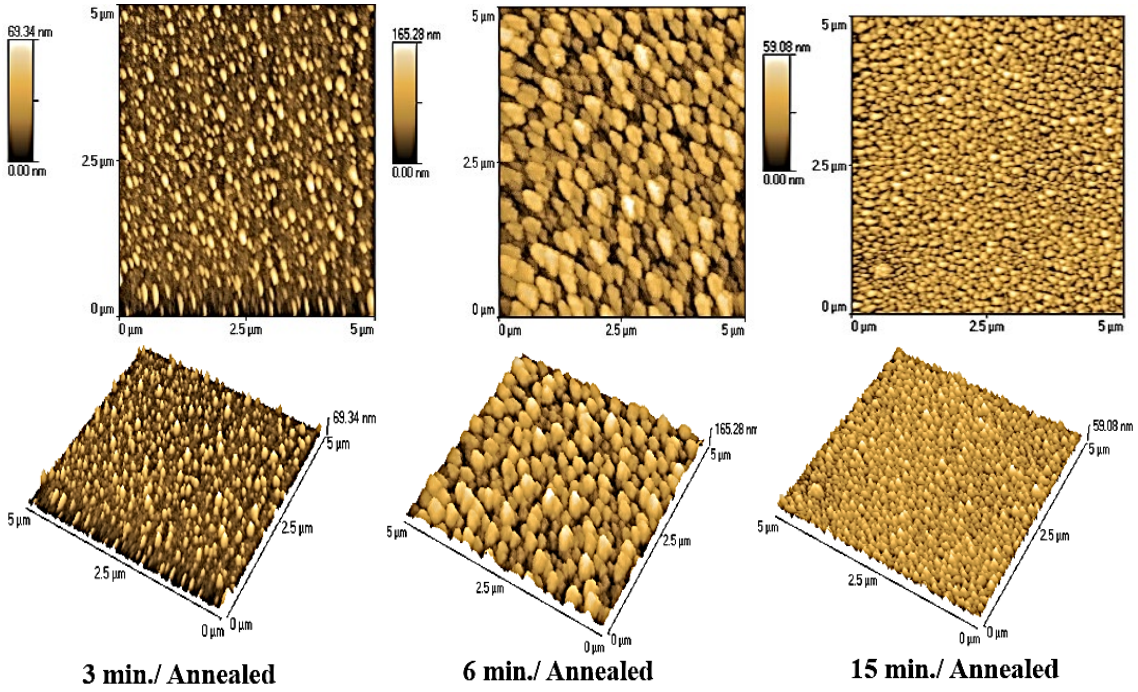

Fig. 7. AFM topographs (in two- and three-dimension view) of post-annealed CATS films.

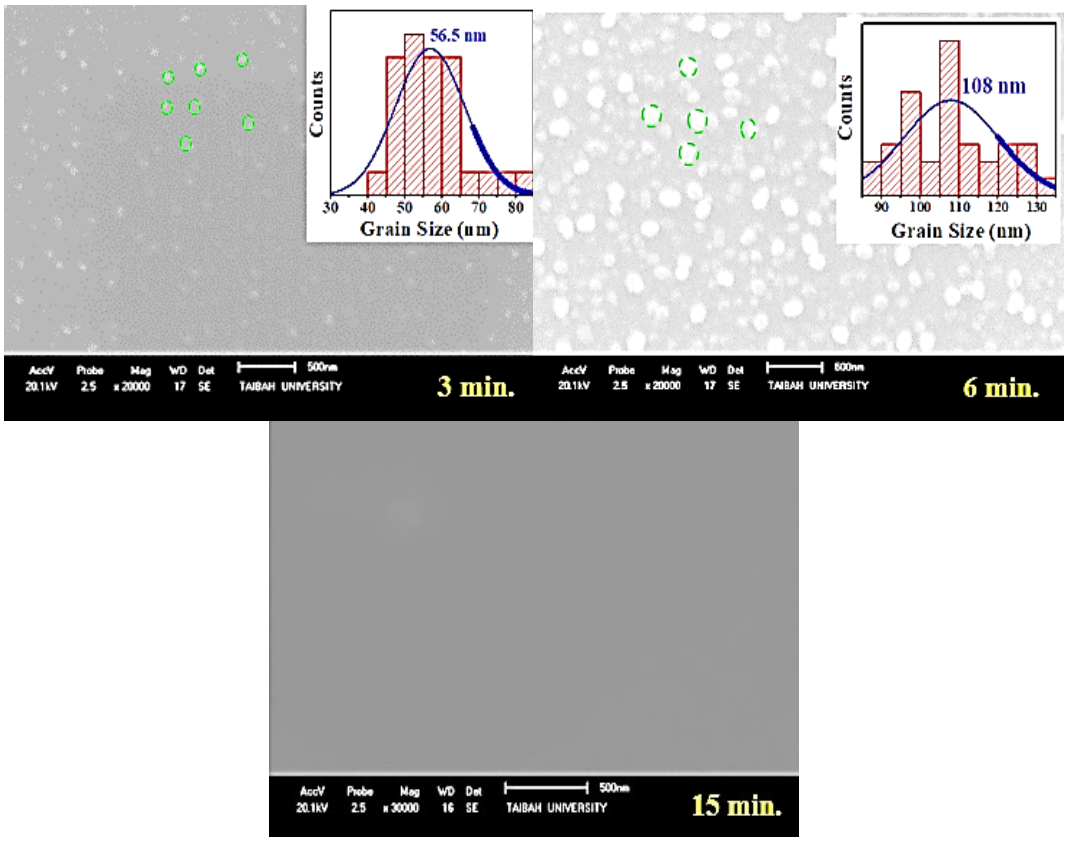

Fig. 8. The SEM images of the as-deposited CATS thin films (Insets: the mean grain size distribution).

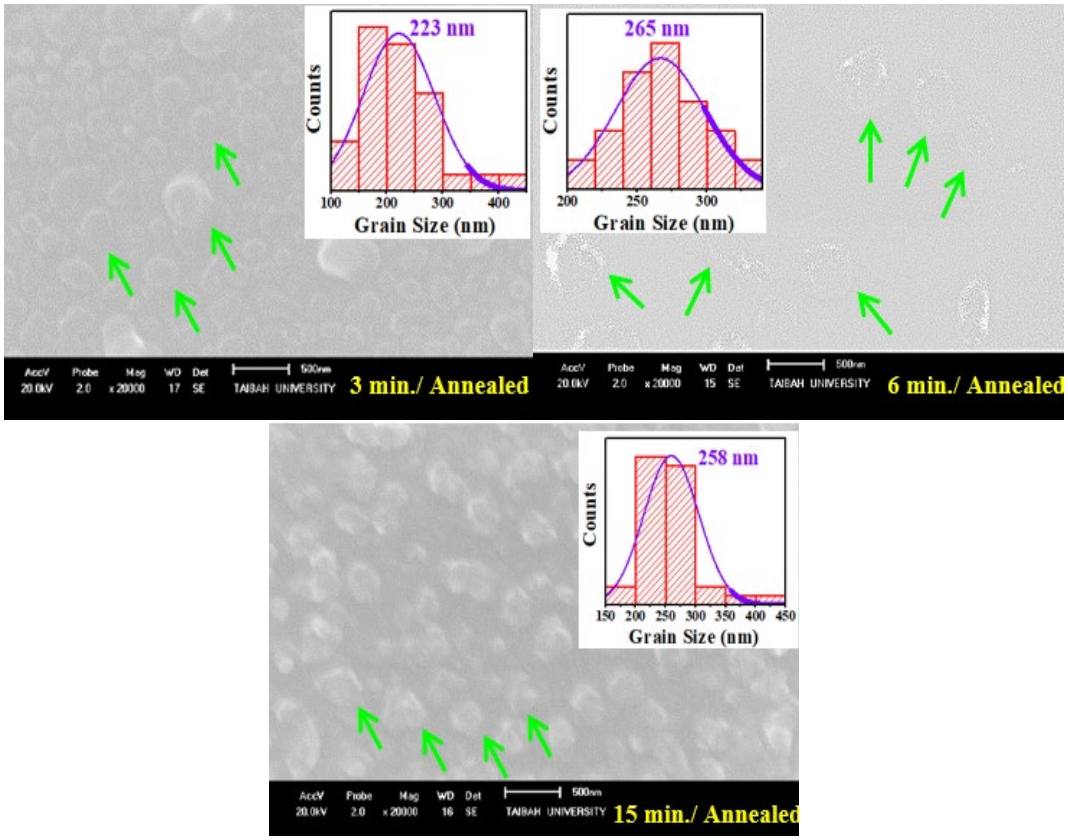

Fig. 9. The SEM images of the annealed CATS thin films (Insets: the mean grain size distribution).

3.4. Optical properties of CATS films

Figs. 10 and 11 show the optical transmission spectra of the CATS films before and after being annealed, respectively. The overall spectral pattern did not reveal any significant change due to the allowed absorption except at the absorbance edges in the optical band gaps (E_g). For all the grown films, Tauc plots ($(\alpha h\nu)^{1/r}$ versus photon energy ($h\nu$)) were generated to determine the values of E_g. The absorption coefficient (α) is related to E_g via [43]:

$$\alpha = \frac{B(h\nu - E_g)^r}{h\nu} \quad (1)$$

where r cas take a value of 0.5 for the direct and 2.0 for indirect allowed electronic transitions across the films forbidden energy gaps. The films optical transmittance (T) and thickness (d) can be related to α via:

$$\alpha = -\frac{1}{d}\ln T \quad (2)$$

The as deposited films at 3, 6 and 15 min attained the thickness of 175, 275 and 341 nm.

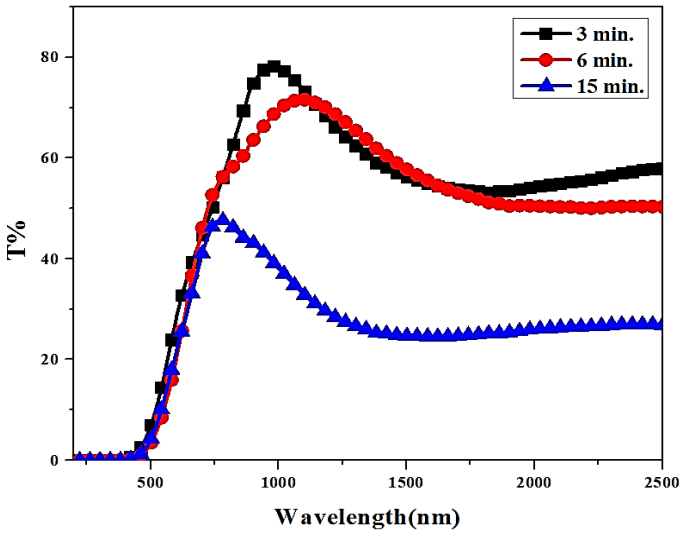

Fig. 10. Optical transmittance of as deposited CATS thin films.

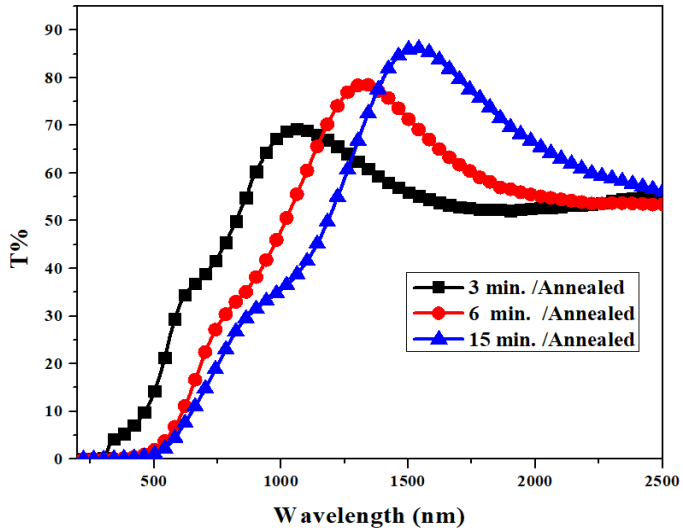

Fig. 11. Transmission spectrum of post-annealed CATS thin film.

Figs. 12 and 13 display the Tauc plots of the as deposited and post-annealed CATS films, respectively. Table 3 shows the obtained E_g values of the films which agreed well with other reports [27, 28, 42, 44]. The values of the E_g were found to be affected by the deposition time variation and the annealing process. These results suggested that the EBD technique can be effective to grow CATS films with desired attributes advantageous for solar cells manufacturing.

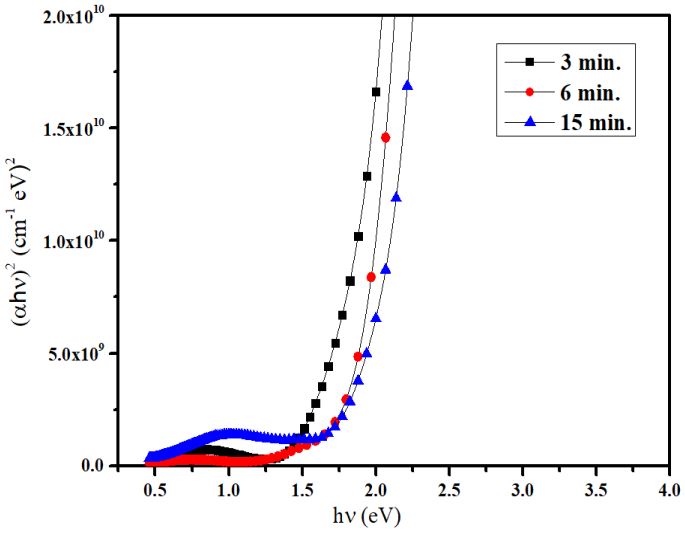

Fig. 12. Tauc plots of as deposited CATS films.

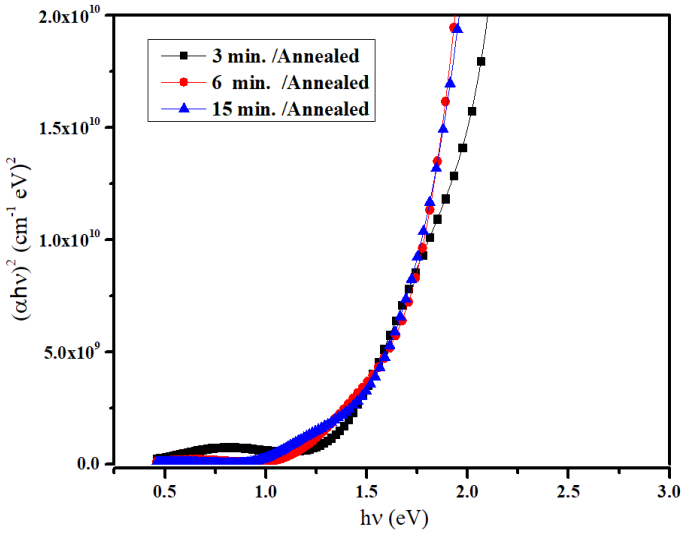

Fig. 13. Tauc plots of post-annealed CATS films.

Figs. 14 and 15 show the Urbach energy (E_u) plots of the as-deposited and post-annealed CATS films. Table 3 displays the achieved values of Eu for the proposed CATS films. The relatively high value of E_u indicated the presence of disorders and impurities in the films. Furthermore, the established inverse correlation between E_u and E_g signified the existence of very less number of localized energy levels in the forbidden energy gap [43].

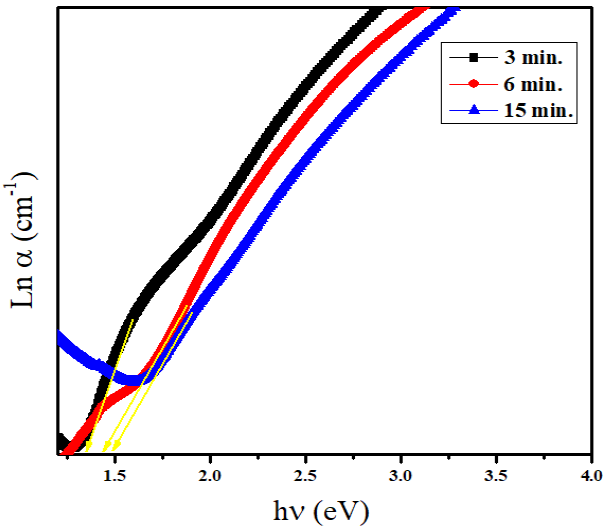

Fig. 14. Urbach plots of the as-deposited CATS films.

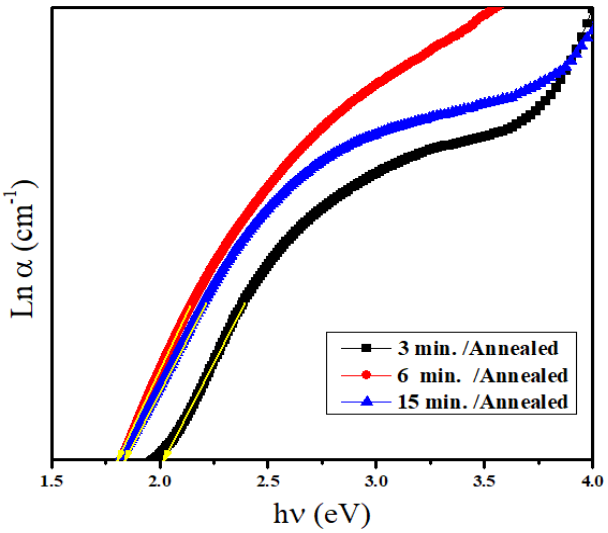

Fig. 15. Urbach plots of the post-annealed CATS films.

Table 3. Calculated values of E_g and E_u of the grown as deposited and post-annealed films.

	As- deposited thin films				**Post-annealed thin films**		
	3 min	6 min	15 min		3 min	6 min	15 min
E_g (eV)	1.26	1.28	1.59		1.14	1.01	0.94
E_u (eV)	0.74	0.69	0.66		0.49	0.55	0.54

4. Conclusions

Three CATS thin films with high purity were prepared by EBD method and characterized. The impact of annealing temperature (450 °C) and various deposition times (3, 6 and 15 min) on the film's structures, morphologies and optical characteristics were determined. It was asserted that the deposition time variation and annealing process can effectively be used to customize the films structures, morphologies, and electronic properties (band gaps). EDX spectrum revealed the occurrence of all constituents in the CATS films. The formation of tetragonal Cu_2AlSnS_4 structure

was validated through the XRD analysis. AFM and SEM images displayed the nucleation of hemispherical grains on the films surface. An inverse relationship between E_g and E_u was obtained. In addition, the salient features of the proposed CATS films were discerned to be comparable to the CTZS films, indicating their immense benefits towards the growth of light-weight and inexpensive photovoltaic devices.

Acknowledgements

The authors appreciate Princess Nourah bint Abdulrahman University Researchers Supporting Project number (PNURSP2025R479), Princess Nourah bint Abdulrahman University, Riyadh, Saudi Arabia.

Funding declaration

The authors declare that no funds, grants, or other support were received during the preparation of this manuscript.

References

[1] Tanaka K, Okamura K, Saito R, et al., J. Mater. Sci. Mater. Electron., 2023.34 (25):1742; https://doi.org/10.1007/s10854-023-11155-6

[2] Bhise SM, Shelke HD, Al-Ahmed A, et al., J. Mater. Sci. Mater. Electron., 2024.35 (19):1304; https://doi.org/10.1007/s10854-024-12988-5

[3] Raval J, Shah B, Kumar D, et al., Chem. Eng. Sci., 2024.119728; https://doi.org/10.1016/j.ces.2024.119728

[4] Fernandes PA, Salomé PMP, Cunha AFD, J. Phys. D. Appl. Phys., 2010.43 (21); https://doi.org/10.1088/0022-3727/43/21/215403

[5] De Wild J, Robert EVC, El Adib B, et al., Sol. Energy Mater. Sol. Cells, 2016.157 (July):259-265; https://doi.org/10.1016/j.solmat.2016.04.039

[6] Dong Y, Lu X, Shen P, et al., Mater. Sci. Semicond. Process., 2018.84 (January):124-130; https://doi.org/10.1016/j.mssp.2018.05.012

[7] Guc M, Oliva F, Fairbrother A, et al., Scr. Mater., 2020.186180-184; https://doi.org/10.1016/j.scriptamat.2020.05.050

[8] Basak A, Deka H, Mondal A, et al., Vacuum, 2018.156298-301; https://doi.org/10.1016/j.vacuum.2018.07.049

[9] Yang G, Li X, Ji X, et al., Sol. Energy, 2020.208 (June):206-211; https://doi.org/10.1016/j.solener.2020.07.090

[10] Minnam Reddy VR, Pallavolu MR, Guddeti PR, et al., J. Ind. Eng. Chem., 2019.7639-74; https://doi.org/10.1016/j.jiec.2019.03.035

[11] Technology E. Optimization Of Monoclinic Cu2SnS3 (CTS) Thin Film Solar Cell Performances Through Numerical Analysis Department of Electrical and Electronic Engineering, Dhaka University of 2020.17 (2):85-98; https://doi.org/10.15251/CL.2020.172.85

[12] Hossain ES, Chelvanathan P, Shahahmadi SA, et al., Chalcogenide Lett., 2018.15 (10):499-507.

[13] Kuku TA, Fakolujo OA, Sol. Energy Mater., 1987.16 (1-3):199-204; https://doi.org/10.1016/0165-1633(87)90019-0

[14] Suryawanshi MP, Ghorpade U V., Shin SW, et al., ACS Appl. Mater. Interfaces, 2016.8 (18):11603-11614; https://doi.org/10.1021/acsami.6b02167

[15] Dias S, Murali B, Krupanidhi SB, Mater. Chem. Phys., 2015.167309-314; https://doi.org/10.1016/j.matchemphys.2015.10.049

[16] Onoda M, Chen XA, Sato A, et al., Mater. Res. Bull., 2000.35 (9):1563-1570; https://doi.org/10.1016/S0025-5408(00)00347-0

[17] Amlouk A, Boubaker K, Amlouk M., Vacuum, 2010.85 (1):60-64; https://doi.org/10.1016/j.vacuum.2010.04.002

[18] Wu C, Hu Z, Wang C, et al., Appl. Phys. Lett., 2007.91 (14):2005-2008; https://doi.org/10.1063/1.2790491

[19] Ghorpade U V., Suryawanshi MP, Shin SW, et al., Chem. Mater., 2016.28 (10):3308-3317; https://doi.org/10.1021/acs.chemmater.6b00176

[20] Mitzi DB, Gunawan O, Todorov TK, et al., Sol. Energy Mater. Sol. Cells, 2011.95 (6):1421-1436; https://doi.org/10.1016/j.solmat.2010.11.028

[21] Avellaneda D, Nair MTS, Nair PK, J. Electrochem. Soc., 2010.157 (6):D346; https://doi.org/10.1149/1.3384660

[22] Kanai A, Toyonaga K, Chino K, et al., Jpn. J. Appl. Phys., 2015.54 (8):3-7; https://doi.org/10.7567/JJAP.54.08KC06

[23] Chantana J, Suzuki K, Minemoto T., Sol. Energy Mater. Sol. Cells, 2017.168 (January):207-213; https://doi.org/10.1016/j.solmat.2017.04.040

[24] Umehara M, Tajima S, Aoki Y, et al., Appl. Phys. Express, 2016.9 (7); https://doi.org/10.7567/APEX.9.072301

[25] Yan C, Huang J, Sun K, et al., Nat. energy, 2018.3 (9):764-772; https://doi.org/10.1038/s41560-018-0206-0

[26] Shockley W, Queisser HJ, J. Appl. Phys., 1961.32 (3):510-519; https://doi.org/10.1063/1.1736034

[27] Timoumi A, Alamri SN, Alsalmi OH, et al., J. Inorg. Organomet. Polym. Mater., 2023.33 (10):3146-3156; https://doi.org/10.1007/s10904-023-02729-2

[28] Timoumi A, Guesmi N El, Alsalmi SNAOH, J. Inorg. Organomet. Polym. Mater., 2023.4 (0123456789); https://doi.org/10.1007/s10904-023-02582-3

[29] Rahman MR, Mia MNH, Uddin MN, et al., J. Mater. Sci. Mater. Electron., 2024.35 (24):1618; https://doi.org/10.1007/s10854-024-13328-3

[30] de Melo Monteiro Modesto AP, Merlo RB, Guzman DG, et al., MRS Adv., 2024.9 (11):916-920; https://doi.org/10.1557/s43580-024-00873-6

[31] El hafidi Z, Outaleb N, Naimi Y., MRS Energy Sustain., 2024; https://doi.org/10.1557/s43581-024-00110-5

[32] Benali H, Hartiti B, Lmai F, et al., Mater. today Proc., 2024; https://doi.org/10.1016/j.matpr.2024.06.012

[33] Khan MT, Prasad KH, Khan A, et al., Inorg. Chem. Commun., 2024.169112973; https://doi.org/10.1016/j.inoche.2024.112973

[34] Courel M, Andrade-Arvizu JA, Guillén-Cervantes A, et al., Mater. Des., 2017.114515-520; https://doi.org/10.1016/j.matdes.2016.10.068

[35] Srinivasa Reddy T, Amiruddin R, Santhosh Kumar MC, Sol. Energy Mater. Sol. Cells, 2015.143 (January 2015):128-134; https://doi.org/10.1016/j.solmat.2015.06.049

[36] Patterson AL, Phys. Rev., 1939.56 (10):978-982; https://doi.org/10.1103/PhysRev.56.978

[37] Adelifard M, Bagheri Mohagheghi MM, Eshghi H, Phys. Scr., 2012.85 (3); https://doi.org/10.1088/0031-8949/85/03/035603

[38] Correa JM, Becerra RA, Ramírez AA, et al., EPJ Photovoltaics, 2016.7 (May 2019); https://doi.org/10.1051/epjpv/2016005

[39] Zhang L, Fang J, Li M, et al., J. Korean Phys. Soc., 2014.64 (3):410-414; https://doi.org/10.3938/jkps.64.410

[40] Julien C, Mavi HS, Jain KP, et al., Mater. Sci. Eng. B, 1994.23 (2):98-104; https://doi.org/10.1016/0921-5107(94)90341-7

[41] Timoumi A, Alzahrani R, Alsherif G, J. Mater. Sci. Mater. Electron., 2023.34 (14):1138; https://doi.org/10.1007/s10854-023-10509-4

[42] Altalhi ATR, Alamri OHASN, Ahmed SA. Novel Synthestic, J. Inorg. Organomet. Polym. Mater., 2023.2 (0123456789)

[43] Mott NF, Davis EA, Philos. Mag., 1970.22 (179):903-922; https://doi.org/10.1080/14786437008221061

[44] Alamri S, Khushaim M, Alamri S, J. Alloys Compd., 2021.870 (March); https://doi.org/10.1016/j.jallcom.2021.159392